Hindawi
Bioinorganic Chemistry and Applications
Volume 2021, Article ID 4018843, 15 pages
https://doi.org/10.1155/2021/4018843

Research Article

A Physical-Chemical Study of the Interference of Ceftriaxone Antibiotic with Copper Chloride Salt

Elsayed M. AbouElleef,[1,2] **Mowafak M. Mahrouka**,[1] **and Sherine E. Salem**[3]

[1]*Chemistry Department, Faculty of Arts and Science, Rafha Northern Border University, 91911 Rafha, Saudi Arabia*
[2]*Basic Science Department, Delta Higher Institute for Engineering and Technology, Mansoura,, 35681 Dakhlia, Egypt*
[3]*Chemistry Department, Faculty of Science, Mansoura University, 35516 Mansoura, Egypt*

Correspondence should be addressed to Elsayed M. AbouElleef; s.abouelleef@yahoo.com

Received 7 August 2021; Revised 2 October 2021; Accepted 6 October 2021; Published 19 October 2021

Academic Editor: Guillermo Mendoza-Diaz

The nano-$CuCl_2.2H_2O$ salt was prepared by the ball milling method. The association parameters for bulk and nano-$CuCl_2$ salts in H_2O are estimated at different temperatures using the conductivity method by applying the Fuoss–Shedlovsky equation and it was higher for nano-$CuCl_2$ than bulk $CuCl_2$ salt. The interaction between the cation (Cu^{2+}) and ligand (ceftriaxone) in H_2O was determined also by the conductometric method. Two stoichiometric complexes 1/2 and 1/1 (M/L) are estimated and follow the order K_f (1/1) > K_f (1 : 2) and ΔG_f (1/1) > ΔG_f (1/2) for (M : L) (in negative values) indicate the favorable of formation of (1/1) complex compared to the (1 : 2) complex. The Gibbs free energies change was increased in negative signs with increasing the temperature. The antimicrobial activities of CFT, bulk Cu-CFT complex, and nano-Cu-CFT complex were studied on LB agar by the disc diffusion technique against clinical isolates of gram-negative bacteria (*Klebsiella pneumonia* and *Pseudomonas aeruginosa*) and Fungi (*Candida albicans*). It was observed that (CFT) has a higher zone of inhibition and antibacterial activity than that of bulk and nano-Cu-CFT complexes in *Klebsiella pneumonia* and *Pseudomonas aeruginosa* (gram-negative bacteria). The nano-Cu-CFT complex showed a higher clear zone of inhibition and antifungal activity against candida than bulk Cu-CFT complex while the absence of the inhibition zone in CFT, so nano-Cu-CFT complex, can be used as an antifungal drug.

1. Introduction

Nanoparticles (NPs) are a wide class of materials that have a state between bulk and atomic or molecular structures in different shapes of 0D, 1D, 2D, or 3D and have a great scientific interest [1–5]. Bulk materials have constant physical properties, with size larger than one micrometer or micron. Nanoparticles can be used for various applications such as drug delivery purposes [6], diagnostics of cancer therapy, gene delivery purposes, chemical and biological sensing [7], gas sensing [8–10], CO_2 capturing [11, 12], and other related applications [13–17]. Nanoparticles are often used to photocatalytically break down oil into biodegradable compounds, break down volatile organic pollutants in the air, and clean up carbon tetrachloride pollution in spring water [18, 19]. Nanoparticles (NPs) such as gold, silver, platinum, and palladium showed colors with the variation of shape and size and characteristic properties that can be utilized in bioimaging applications [20]. Another application of nanoparticles is the synthesis of photocatalysis S-doped TiO_2 nanoparticles and the study of their photocatalytic, antimicrobial, and antioxidant activities under sunlight illumination [21].

Ceftriaxone [22–25] is an antibiotic that belongs to a category of medicine referred to as cephalosporin antibiotics, and it treats a variety of bacterial infections by stopping the growth of bacteria variety of bacterial infections (e.g., middle ear, lower tract, skin, and urinary tract), meningitis, gonorrhea, pelvic disease, and joint infections.

Thermodynamics parameters are an important tool for learning about the spontaneity of a given process at a particular temperature [26, 27]. Determination of the formation constant is fundamental for understanding the behavior of the metal cations in the presence of some chelating agent in a solution and is best explained using thermodynamics. A conductivity technique can be used to estimate the interaction between the metal cations and the chelating agent by estimating the thermodynamics parameters of metal-ligand complex formation [28–32].

It is therefore necessary to study the effect of antibiotic ceftriaxone on the properties of copper chloride salt by determining thermodynamics parameters of interaction between them using conductometric techniques to find the extent of benefit of the antibiotic ceftriaxone.

2. Experimental

2.1. Materials and Solutions. The purities and sources of the materials used are presented in Table 1. The structure of ceftriaxone is shown in Figure 1.

2.2. Apparatus. The conductance measurements are carried out with a conductometer A JENCO, Vision plus-EC3175 conductance instrument, and connecting with Kottermann ultra-thermostat-4130 (a deviation ±0.01 K) with a cell constant equal unity. The conductivity bridge was calibrated using standard potassium chloride solutions [33].

The Bruker D_8 Advance X-ray diffractometer is a powder XRD instrument used to record X-ray diffraction (XRD) patterns of bulk and nanosamples. The Bruker diffractometer with CuKα anode radiation ($\lambda = 0.1542$ nm) as a source is operating at 40 kV and 30 mA. The scanning range of over an angular range was between 4° and 80°A at a temperature of 25°C, and the scan mode was applied with a step width of 0.02° per step and step time of 0.4 s.

IR instrument of the type Thermo Scientific Nicolet iS10 FTIR spectrometer is operating in the spectral range of 7800 to 400 cm^{-1} with a resolution of 4 cm^{-1}, midinfrared KBr beamsplitter 4000 to 400 cm^{-1}.

Solid samples can be prepared by grinding about 5 mg of sample mixed with 100 mg of spectroscopic grade KBr. This powder mixture is then compressed into a pellet using a mechanical press between 4 and 8 ton.cm^{-2} for 2 minutes in the form of 10 mm in diameter disks to form a translucent (http://en.wikipedia.org/wiki/Infrared_spectroscopy%20-%20cite_note-Har-2).

2.3. Procedure

2.3.1. Preparation of Nanocopper Chloride. The nano-$CuCl_2.2H_2O$ salt was prepared by the ball milling method by shaking $CuCl_2.2H_2O$ salt in ball milling apparatus of the type Retsch MM 2000 swing mill at 20225 Hz at room temperature for one hour. The mill has 10 cm^3 stainless steel double-walled tubes. Two balls made from stainless steel of 12 mm diameter were used.

2.3.2. Preparation of Bulk Cu-CFT Complex and Nano-Cu-CFT Complex. Bulk Cu-CFT complex and nano-Cu-CFT were prepared according to a traditional method by refluxing 1 mmol of CFT under investigation with 1 mmol of bulk $CuCl_2.2H_2O$ or nano-$CuCl_2.2H_2O$ salts in an ethanolic solution for 2-3 h close to the boiling point of the solvent. The precipitate was filtered off, washed several times with absolute ethanol, and finally dried in vacuum desiccators over anhydrous calcium chloride.

2.3.3. Conductance Measurements. To calculate the association parameters of $CuCl_2.2H_2O$ solutions, a solution of metal cation (10^{-3} M, 20 mL) was placed in a double jacket glass conductance cell, and the conductance was measured after each addition of the solvent and stirring at a specific temperature.

To calculate the formation constants between $CuCl_2.2H_2O$ and a ligand (ceftriaxone) in the solvents, a solution of $CuCl_2.2H_2O$ (10^{-3} M, 20 mL) was placed in a conductance cell, and the conductance was measured. The ligand (10^{-3} M) (ceftriaxone) was added step by step to the conductance cell using a micropipette and the conductance was measured after each addition.

2.3.4. Biological Activity. The antimicrobial activities of CFT, bulk Cu-CFT complex, and nano-Cu-CFT complex were studied on LB agar by the disc diffusion technique against clinical isolates of gram-negative bacteria (*Klebsiella pneumonia* and *Pseudomonas aeruginosa)* and fungi (*Candida albicans*).

Sterile filter paper discs (6 mm) were individually immersed in dimethyl sulfoxide (DMSO) extract of CFT, bulk Cu-CFT complex, and nano-Cu-CFT complex, and DMSO was used as control. All the discs were dried, placed on the surface of the test bacterial and fungal, and incubated for 18 to 24 h at 37°C. The standard antibiotic used is ceftazidime (30 mg) and finally, the zones of inhibition were examined.

3. Results and Discussion

3.1. X-Ray Diffraction (XRD). The X-ray diffraction (XRD) pattern for the bulk and nano-$CuCl_2.2H_2O$ salt is shown in Figure 2. The positions of the main peaks and their relative intensities as measured by powder diffraction are listed in Table 2.

The mean size of nanocrystals was determined from the diffraction peaks corresponding to the most intensive reflections according to the Joint Committee on Powder Diffraction Standards database. Scherrer's equation was used to determine the average crystallite size for nanoparticles from the XRD diffraction pattern measured [34, 35]:

$$d = \frac{K\lambda}{\beta \cos \theta}, \quad (1)$$

where K is Scherrer's constant (about 0.9), λ is the wavelength ($\lambda = 0.154$ nm), β is the line broadening at half the maximum intensity in radians, θ is the Bragg angle, and d is the averaged dimension of crystallites in nanometers. Groth

Table 1: Sources and purity of the materials.

Chemical name	CAS reg. no.	Mass fraction	Purification method	Suppliers
Ceftriaxone	104376-79-6	0.990	Used as received	Sigma-Aldrich
Ethanol	64-17-5	0.995	Used as received	Sigma-Aldrich
$CuCl_2{\cdot}2H_2O$	13464-92-1	0.980	Used as received	Sigma-Aldrich
H_2O	7732-18-5	$k < 0.5\,\mu S{\cdot}cm^{-1}$	Distillation	Our lab

Mass fraction purity was provided by the suppliers.

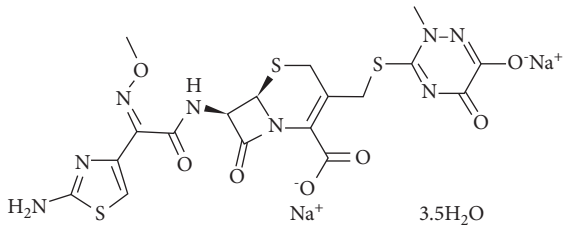

Formula $C_{18}H_{16}N_8Na_2O_7S_3.3.5H_2O$
Molar mass 598.54 g/mol

Figure 1: Molecular structure of ceftriaxone antibiotic (CFT). Formula: $C_{18}H_{16}N_8Na_2O_7S_3.3.5H_2O$. Molar mass: 598.54 g/mol.

assigned $CuCl_2{\cdot}2H_2O$ to the bipyramidal class of the orthorhombic crystalline system with the axial ratios $a:b:c = 0.9179:1:0.4627$. Layer line measurements give the identity distances $a_0 = 7.38$ Å, $b_0 = 8.04$ Å, $c_0 = 3.72$ Å. These lead to the ratios $a:b:c = 0.918:1:0.462$, in good agreement with the crystallographic data [36]. The mean crystal size (nm) of bulk and nano-$CuCl_2{\cdot}2H_2O$ salts obtained by XRD are mentioned in Table 2 [37].

A little difference was observed between bulk and nanosalts in peaks other than their intensities. Also, it was found that the salt remains in the crystalline form by converting it to nanoparticles. The main difference between the bulk and nanosalt was in the crystal size, as shown in Table 3.

3.2. Infrared Analysis (IR). Infrared spectra (IR) were used to identify the structure of ceftriaxone (CFT), as shown in Figure 3, and its complexes with bulk and nano-$CuCl_2.2H_2O$ salts as their functional groups give rise to characteristic bands in terms of both intensity and position (frequency), as shown in Figures 4 and 5.

It was observed from the IR spectra of ceftriaxone (CFT) ligand that amidic N-H stretching vibrations mean strong intensity bands occurring at 3440 and 3261 cm^{-1} are due to N-H asymmetric and symmetric stretching, respectively [38]. Amidic C=O stretching vibrations mean a strong intensity band identified at 1649 cm^{-1} is due to C=O stretching vibrations [38]. Amidic N-H deformation and C-N stretching mean the strong bands observed at 1608, 1537, and 1500 cm^{-1} are due to amide N-H deformation vibrations [38, 39]. C-H stretching vibrations mean the weak bands occurring at 2891 cm^{-1} are assigned to CH_3 symmetric stretching. The bands appearing at 2934 cm^{-1} in the IR spectra are due to CH_3 asymmetric stretching vibrations [40]. C-H deformation vibrations mean the weak bands observed at 822, 804, and 730 cm^{-1} are allotted as C-H out-of-plane deformation vibrations and medium-to-weak intensity bands present at 1104 and 1033 cm^{-1} are allotted as C-H in plane deformation vibrations. A strong band occurring at 1399 cm^{-1} is due to the -CH_2- deformation vibration. Weak bands present at 1243 and 760 cm^{-1} are due to CH_2 wagging and CH_2 rocking vibrations, respectively [40]. Lactam C=O stretching vibrations mean a strong band observed at 1741 cm^{-1} in the IR spectrum of ceftriaxone is allotted to be due to C=O stretching vibration [41]. C-O-C stretching vibrations mean strong bands present at 1033 and 1243 cm^{-1} are assigned as C-O-C symmetric and asymmetric stretching vibrations, respectively [41]. C-S stretching vibrations mean weak bands observed at 646 and 616 cm^{-1} are due to C-S stretching vibrations [42]. C-N stretching vibrations mean the medium band present at 1285 cm^{-1}, weak band at 1243 cm^{-1}, and medium band present at 1185 cm^{-1} are due to C-N stretching vibrations. C=C and C=N stretching vibrations mean very strong intensity bands present at 1608, 1537, and 1500 cm^{-1} are assigned to C=C and C=N stretching vibrations [43]. O-H stretching vibrations mean strong intensity bands identified at 3440 and 3261 cm^{-1} are allotted as O-H stretching vibrations [44]. C-C and C-C-C bending vibrations mean a very weak band occurring at 507 cm^{-1} in is due to C-C out-of-plane bending vibrations. The weak bands occurring at 646 and 606 cm^{-1} are due to C-C-C in plane and out of plane deformation vibrations, respectively [45].

In the IR spectra of bulk Cu-CFT complex, as shown in Figure 4, after ceftriaxone coordination to copper ion, the frequencies of the (C=O) lactam shifted from 1741 cm^{-1} to higher wavenumber 1775 cm^{-1}, one amidic (C=O) shifted from 1649 to lower wavenumber 1624 cm^{-1}, and also another amidic (C=O) triazine shifted from 1608 to lower wavenumber 1553 cm^{-1}. There are three functional groups participating in the formation of a complex. The increase in the vibrational frequencies of carbonyl groups can be explained by oxygen of lactam and triazine coordinating to Cu(II) indicates the formation of a chelate complex [46, 47]. These intramolecular interactions between oxygen and copper ion result in a more rigid molecular structure around the oxygen and shift of carbonyl (C=O) vibrational frequencies to higher wavenumbers. The frequency of the symmetric stretching mode ν_s(COO−) shifts from 1391 to 1398 cm^{-1}. These shifts indicate that the carboxylate group (COO), the lactam carbonyl group (C=O), and the oxo group of the triazine ring are involved in the formation of $[Cu(CFT)]{\cdot}3H_2O$. This analysis is in agreement with previous studies where ceftriaxone is described as a polydentate chelating ligand [46, 47]. The broadband in the [Cu(CFT)]·

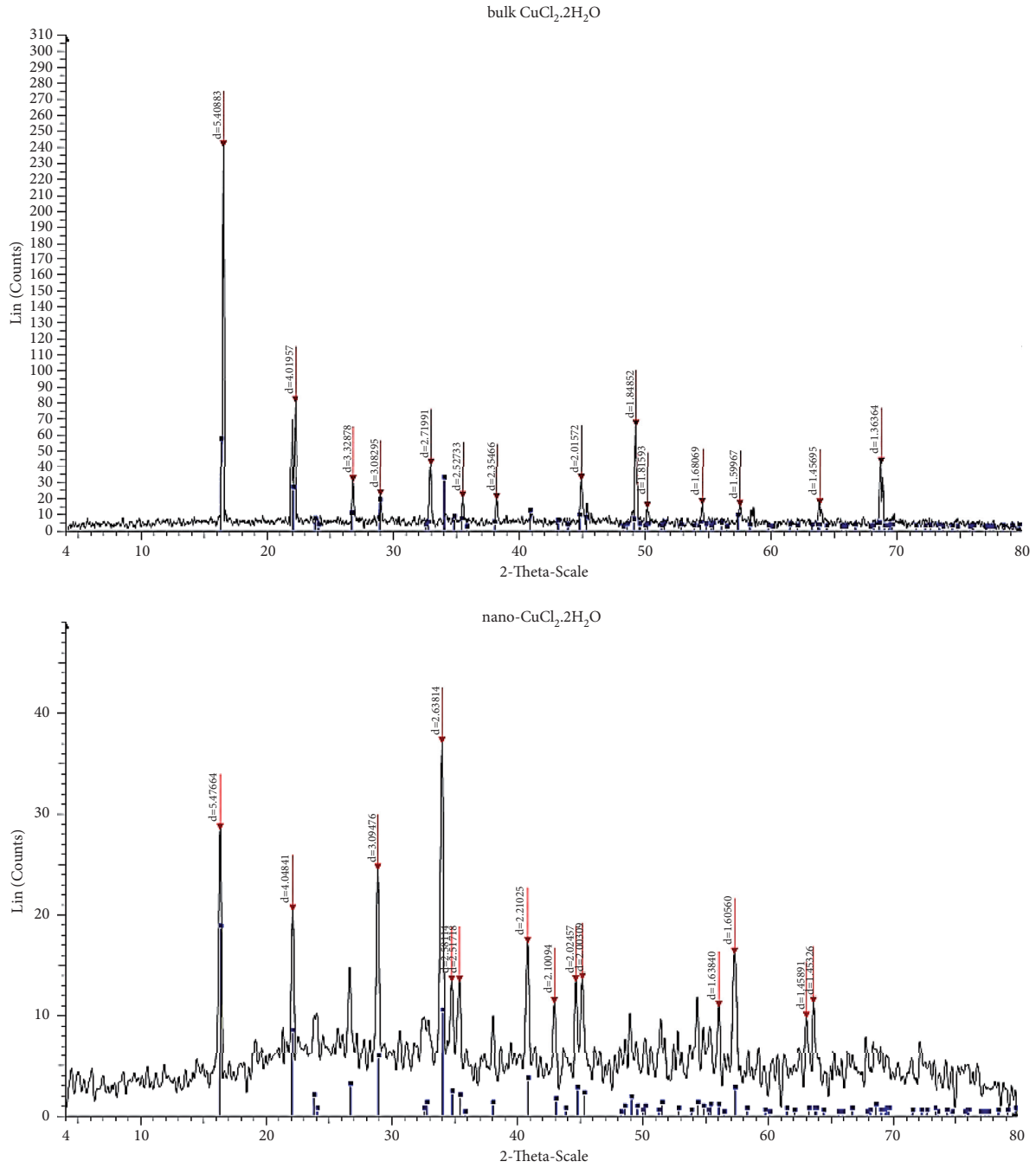

Figure 2: X-Ray diffraction of bulk and nano-$CuCl_2{\cdot}2H_2O$ salt.

Table 2: Intensity (%) and crystal size (nm) of bulk and nano-$CuCl_2.2H_2O$ salt.

Bulk $CuCl_200B72H_2O$ salt					Nano-$CuCl_2{\cdot}2H_2O$ salt				
Angle (2-theta °)	d value (angstrom)	Intensity (count)	Intensity %	Crystal size (nm)	Angle (2-theta °)	d value (angstrom)	Intensity (count)	Intensity %	Crystal size (nm)
16.375	5.40883	241	100	158.2	16.171	5.47654	28.5	76.8	16.171
22.097	4.01957	80	33.2	58.4	21.937	4.04841	20.4	55	21.937
26.76	3.32876	29.9	12.4	101.5	28.825	3.09476	24.5	65.9	28.825
28.938	3.08295	21.2	8.8	58.4	33.954	2.63814	37.1	100	33.954
32.916	2.71891	40.8	17	111.3	34.727	2.58114	13.3	35.9	34.727
35.491	2.52733	19.8	8.2	52.1	35.349	2.53715	13.3	35.8	35.349

Table 2: Continued.

Bulk $CuCl_2$00B72H_2O salt					Nano-$CuCl_2$·2H_2O salt				
Angle (2-theta °)	d value (angstrom)	Intensity (count)	Intensity %	Crystal size (nm)	Angle (2-theta °)	d value (angstrom)	Intensity (count)	Intensity %	Crystal size (nm)
38.19	2.35466	18.9	7.8	98.1	40.793	2.21025	17.2	46.3	40.793
44.933	2.01572	30.7	12.7	67.4	43.018	2.10094	11.2	30.1	43.018
49.254	1.84852	65.2	27.1	132.3	44.726	2.02457	13.3	35.9	44.726
50.199	1.81593	13.5	5.6	134.6	45.234	2.00303	13.6	36.5	45.234
54.558	1.68069	15.8	6.6	3	56.088	1.6384	10.8	29.1	56.088
57.572	1.59967	14.6	6.1	107.9	57.343	1.6055	16.1	43.4	57.343
63.915	1.45535	15.4	6.4	140.7	63.208	1.46991	9.72	26.2	63.208
68.788	1.36364	41.6	17.3						

Table 3: Mean crystal size (nm) of bulk and nano-$CuCl_2$·2H_2O salts.

Sample	Crystal size d_{XRD} (nm)
Bulk $CuCl_2$.2H_2O	94.146
Nano-$CuCl_2$.2H_2O	43.98

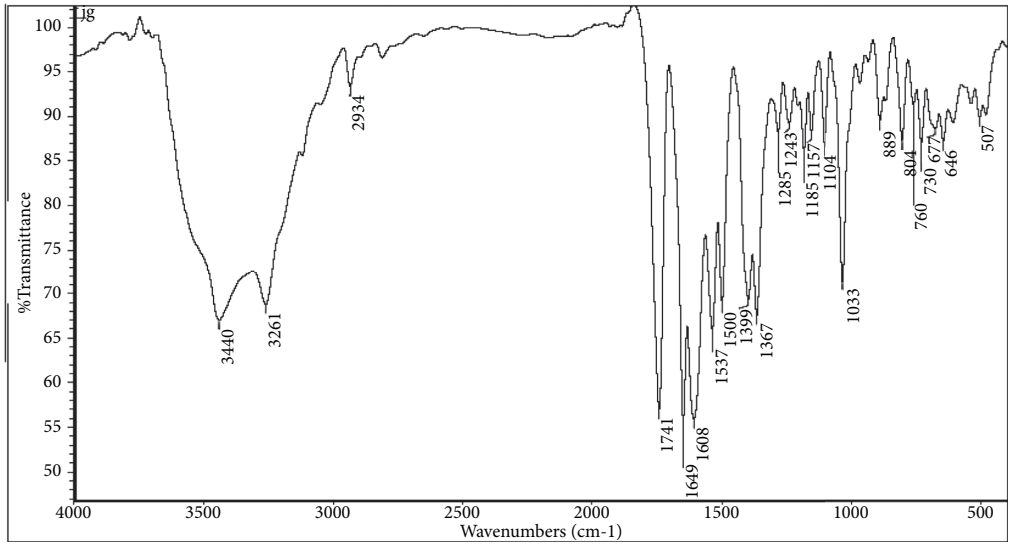

Figure 3: IR spectra of ceftriaxone (CFT).

3H_2O spectrum at 1624 cm^{-1} has a high intensity and a low resolution due to the overlap of several vibrational modes, including ν(C=O)-amide, ν(C=O)-triazine, ν_{as}(COO–), ν(C=C), and ν(C=N). A new band appearing at the frequency 468 cm^{-1} in the complex that is absent in the free ligand is due to ν (Cu-N) stretching vibration also giving strong evidence for the coordination of tertiary nitrogen atom with copper ion [47].

Also, the IR spectra of nano-Cu-CFT complex asym.(NH_2) shifted from 3440 to lower wavenumber 3427 cm^{-1}, carboxylic (-OH) group appeared at wavenumber 2924 cm^{-1}, carboxylic (C=O) appeared at wavenumber 1742 cm^{-1}, one amidic (C=O) shifted from 1649 to lower wavenumber 1638 cm^{-1} and also another amidic (C=O) shifted from 1608 to lower wavenumber 1553 cm^{-1}, as in Figure 5. This indicates the formation of a complex between $CuCl_2$.2H_2O salt and CFT antibiotic.

3.3. Conductometric Measurements

3.3.1. Calculation of Association Parameters for Bulk and Nano-$CuCl_2$·2H_2O Salts in Distillate H_2O. The specific conductance values (K_s) of different concentrations of bulk and nano-$CuCl_2$·2H_2O salt in distillate H_2O were measured experimentally in absence of (CFT) at different temperatures (288.15, 293.15, 298.15, and 303.15 K). The molar conductance (Λ_m) values were calculated [48–50] using

$$\Lambda_m = \frac{(K_s - K_{solv}) \times 1000}{C}, \quad (2)$$

where K_s and K_{solv} are the specific conductance of the solution and the solvent (distillate H_2O), respectively, and C is the concentration of the bulk and nano-$CuCl_2$·2H_2O solutions.

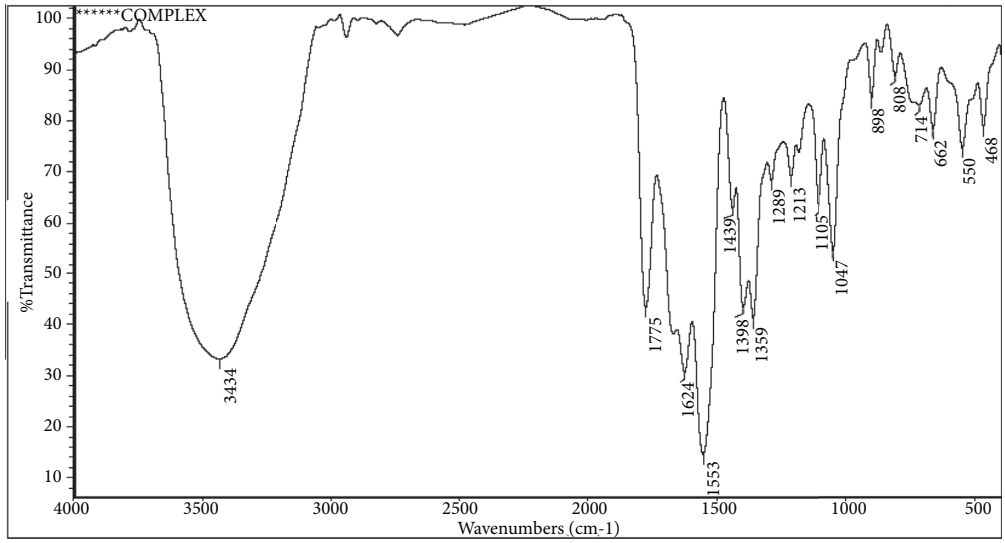

Figure 4: IR spectra of bulk Cu-CFT complex.

The experimental data for conductance measurements were analyzed using Fuoss–Shedlovsky extrapolation techniques [51–53] which follow equations (3)–(12):

$$\frac{1}{\Lambda S_{(Z)}} = \frac{1}{\Lambda_o} + \left(\frac{K_A}{\Lambda_o^2}\right)\left(C\Lambda\gamma_{\pm}^2 S_{(Z)}\right). \tag{3}$$

The results obey the Fuoss–Shedlovsky equation and can be applied to obtain the value of limiting molar conductivity (Λ_o) and association constant (K_A) by plotting a graph between $1/\Lambda S(z)$ and $(C\Lambda S(z)\gamma_{\pm}^2)$, which is presented in Figure 6, giving straight line with intercept ($1/\Lambda_o$) and slope (K_A/Λ_o^2):

$$S_{(Z)} = 1 + Z + \frac{Z^2}{2} + \frac{Z^3}{2} + \ldots, \tag{4}$$

$$Z = \frac{S(\Lambda C)^{1/2}}{\Lambda_0^{3/2}}, \tag{5}$$

$$S = a\Lambda_0 + b, \tag{6}$$

$$a = \frac{8.2 \times 10^5}{(\varepsilon T)^{3/2}}, \qquad b = \frac{82.4}{\eta(\varepsilon T)^{1/2}}, \tag{7}$$

$$(\alpha) = \frac{\Lambda S_{(Z)}}{\Lambda_0}, \tag{8}$$

$$\log \gamma_{\pm} = \frac{-A(\alpha C)^{1/2}}{\left[1 + Br^o(\alpha C)^{1/2}\right]}, \tag{9}$$

$$A = 1.824 \times 10^6 (\varepsilon T)^{-3/2}, \qquad B = 50.29 \times 10^8 (\varepsilon T)^{-1/2}, \tag{10}$$

$$K_A = \frac{C_{[MX_n]} \cdot \gamma_{[MX_n]}}{C_{M^{n+}} \cdot \gamma_{M^{n+}} \cdot C_{X^-}^n \cdot \gamma_{X^-}^n}, \tag{11}$$

where (S) is the Onsager slope; (ε) is the dielectric constant of the solvent, ; (η_o) is the viscosity of the solvent; (T) is the temperature; (α) is the degree of dissociation; ($\gamma_{\pm}$) is the mean activity coefficients; (z^-, z^+) are the charges of ions in solutions; (A, B) are the Debye–Hückel constant; (r^o) is the solvated radius; and (K_A) is the association constant.

The dissociation constant (K_D) is calculated by the following equation:

$$K_D = \frac{1}{K_A}. \tag{12}$$

The Walden product ($\Lambda_o\eta_o$) values were calculated from the values of limiting molar conductance (Λ_o) [54]:

$$\text{Walden product} = \Lambda_o\eta_o. \tag{13}$$

The triple ion association constant K_3 can be calculated from

$$\frac{\Lambda C^{1/2}}{(1 - (\Lambda/\Lambda_o))^{1/2}} = \frac{\Lambda_o}{(K_A)^{1/2}} + \frac{\lambda_3^o C}{K_3 (K_A)^{1/2}}\left(1 - \frac{\Lambda}{\Lambda_o}\right). \tag{14}$$

The values of free energy of association (ΔG_A) of bulk and nano-$CuCl_2.2H_2O$ salt in H_2O at different temperatures of 288.15, 293.15, 298.15, and 303.15 K were calculated from the association constant K_A values [55] by using

$$\Delta G_A = -2.303RT \log K_A. \tag{15}$$

The activation energy of the transfer process can be estimated depending on the relation between conductance of ion, ion mobility, and temperature degree, as in the Arrhenius equation:

$$\Lambda_o = Ae^{-E_a/RT}, \tag{16}$$

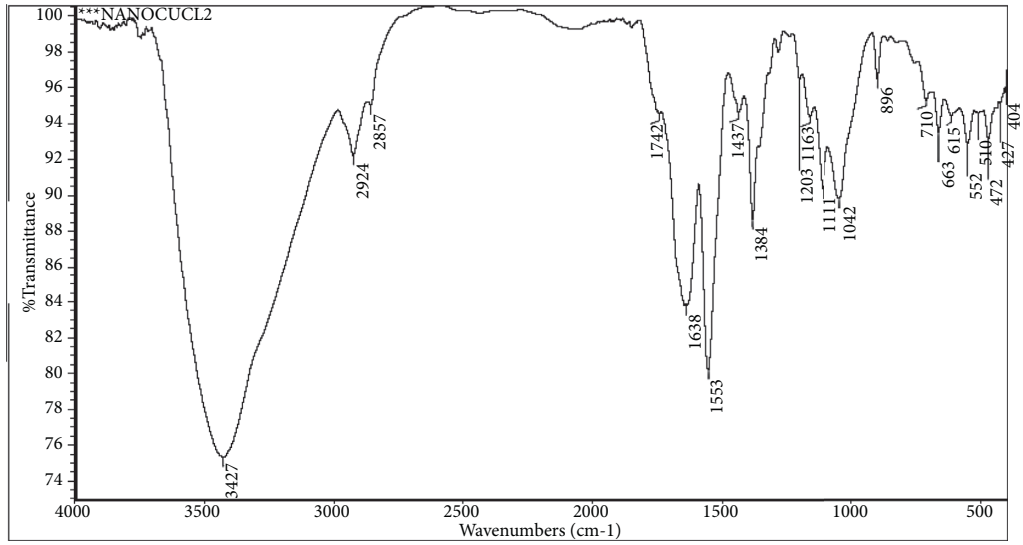

Figure 5: IR spectra of nano-Cu-CFT complex.

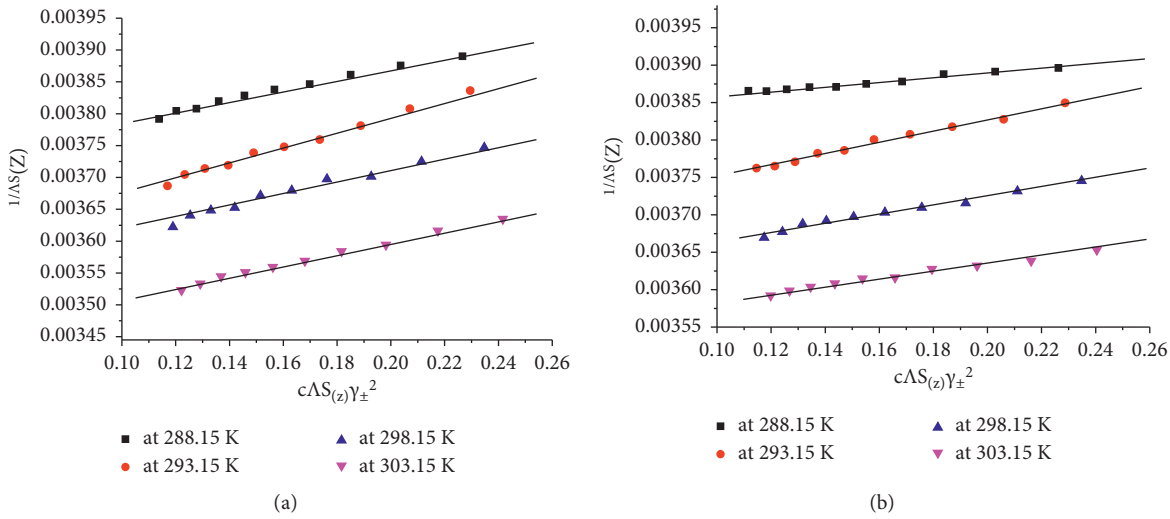

Figure 6: Variation of the molar conductance, $l/\Lambda S_{(z)}$ with $C\Lambda\gamma^2_{\pm}\ S_{(z)}$ for (a) bulk $CuCl_2{\cdot}2H_2O$ and (b) nano-$CuCl_2{\cdot}2H_2O$ in distillate H_2O at (288.15, 293.15, 298.15, and 303.15) K.

where A is the frequency factor and E_a Arrhenius activation energy of the transport process.

$$\log \Lambda_o = \log A - \frac{E_a}{2.303RT}. \tag{17}$$

By plotting log Λ_o versus l/T, as shown in Figure 7, the activation energy of transfer processes values can be calculated from the slope [56].

The calculated values of Λ_o, $S_{(Z)}$, α, $\gamma_{\pm}$, K_A, K_D, and K_3 for the solutions of bulk and nano-$CuCl_2{\cdot}2H_2O$ salt with distillate H_2O at different temperatures of 288.15, 293.15, 298.15, and 303.15 K are calculated and reported in Tables 4 and 5.

Table 4 shows that the limiting molar conductivity (Λ_o) increases with increasing temperature due to the increase in mobility of ions and increasing kinetic energy which increases the separation among the oppositely charged ions while the Walden product ($\Lambda_o\eta$) decreases with increasing the temperature due to the decrease in viscosity; also, the association constant (K_A) decreases with increasing the temperature due to the decrease in the association of ions and the increase in mobility of ions; and similarly, the triple ion association constant (K_3) decreases with increasing the temperature due to the decrease for the same reason.

Table 5 shows the same trend, that is, the limiting molar conductivity (Λ_o) increases with increasing the temperature while the Walden product ($\Lambda_o\eta$) decreases with increasing the temperature; also association constant (K_A) decreases with increasing the temperature; and similarly, the triple ion association constant (K_3) decreases with increasing the temperature.

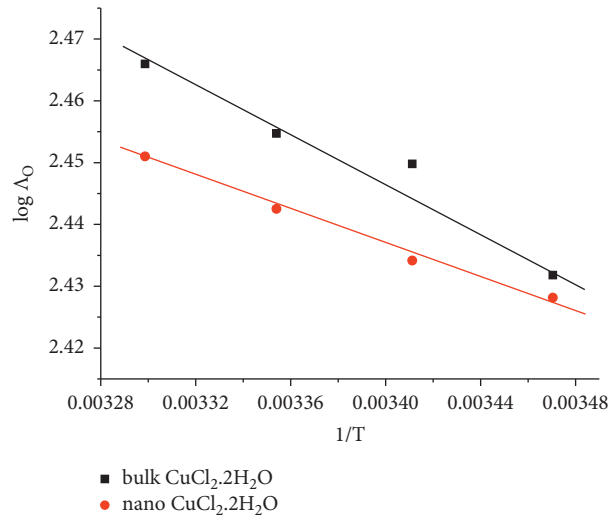

Figure 7: Variation of log Λ_o with l/T (K^{-1}) of for bulk and nano-$CuCl_2{\cdot}2H_2O$ in H_2O.

Table 4: Different association parameters (limiting molar conductance (Λ_o), Fuoss–Shedlovsky parameter $S_{(z)}$, degree of dissociation (α), activity coefficient ($\gamma_\pm$), association constant (K_A), dissociation constant (K_D), triple ion association constant (K_3)) for bulk $CuCl_2{\cdot}2H_2O$ in distillate H_2O at 288.15, 293.15, 298.15, and 303.15 K in absence of CFT.

T (K)	Λ_o S·cm^2·mol^{-1}	$\Lambda_o\eta$ S·cm^2·MPa·s·mol^{-1}	α	$\gamma_\pm$	K_A dm^3·mol^{-1}	$10^{-3}K_D$ mol·dm^{-3}	10^5K_3 (dm^3·mol^{-1})^2
288.15	270.00	307.43	0.9806	0.9022	99.74	0.0100	1.322
293.15	281.69	282.14	0.9668	0.9013	93.39	0.0107	1.273
298.15	284.90	254.16	0.9755	0.9005	82.79	0.0120	1.190
303.15	292.39	233.09	0.9912	0.8995	78.32	0.0127	1.154

Table 5: Different association parameters (limiting molar conductance (Λ_0), Fuoss–Shedlovsky parameter $S_{(z)}$, degree of dissociation (α), activity coefficient ($\gamma_\pm$), association constant (K_A), dissociation constant (K_D), triple ion association constant (K_3)) for nano-$CuCl_2{\cdot}2H_2O$ in distillate H_2O at 288.15, 293.15, 298.15, and 303.15 K in the absence of CFT.

T (K)	Λ_o S·cm^2·mol^{-1}	$\Lambda_o\eta$ S·cm^2·MPa ·s·mol^{-1}	α	$\gamma_\pm$	K_A dm^3·mol^{-1}	$10^{-3}K_D$ mol dm^{-3}	10^5K_3 (dm^3·mol^{-1})^2
288.15	266.21	302.58	0.9754	0.9022	60.60	0.0165	0.9949
293.15	271.73	282.14	0.9013	0.9013	56.35	0.0177	0.9546
298.15	277.00	247.11	0.9873	0.9005	46.16	0.0216	0.8499
303.15	282.48	225.19	0.9874	0.8995	34.47	0.0290	0.0714

The enthalpy (ΔH_A) for bulk and nano-$CuCl_2{\cdot}2H_2O$ salts with distillate H_2O at different temperatures were calculated by using Van 't Hoff equation:

$$\log K = -\frac{\Delta H}{2.303R}\left(\frac{1}{T}\right) + \text{constant}. \quad (18)$$

By drawing the relation between log K_A and 1/T, ΔH_A can be calculated from the slope of each line which equals (-ΔH_A/2.303 R), as shown in Figure 8. The entropy (ΔS_A) for bulk and nano-$CuCl_2{\cdot}2H_2O$ salts were calculated by using

$$\Delta G_A = \Delta H_A - T\Delta S_A, \quad (19)$$

where (S) is the entropy of the system. The calculated values of (ΔH_A) and (ΔS_A) for bulk and nano-$CuCl_2{\cdot}2H_2O$ salts are presented in Table 6. It is obvious that the limiting molar conductance (Λ_o) increased as the temperature increased while the dissociation degree decreased as the temperature increased indicating a higher solvation process. The values of the association constant (K_A) and the triple ion association constant (K_3) were decreased by increasing the temperature. Gibbs free energies change of association (ΔG_A) was decreased with negative signs by increasing the temperature indicating that association is favored with lowering of dielectric constant of solvent mixture. The decrease in the values of activity coefficient, limiting molar conductance, association constant, Gibbs free energy change of association, and Walden product for nano-$CuCl_2{\cdot}2H_2O$ in comparison to bulk $CuCl_2{\cdot}2H_2O$ indicates that the association of nano-$CuCl_2{\cdot}2H_2O$ is greater than bulk $CuCl_2{\cdot}2H_2O$ salt, due to the high surface to volume ratio of nanoparticles which leads to a greater ability for ion-pair formation.

3.3.2. Calculation of Formation Constants for Bulk and Nano-Cu-CFT Complexes in H_2O at Different Temperatures. Different lines were obtained with breaks indicating the formation of (1 : 2) and (1 : 1) (M : L) stoichiometric

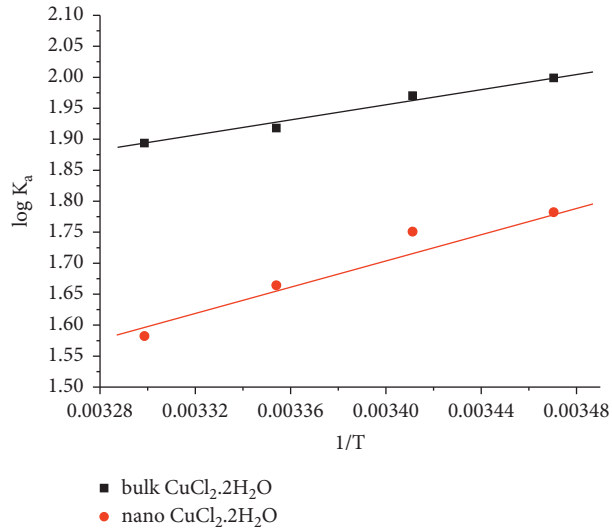

Figure 8: Variation of log K_a with $1/T$ (K^{-1}) of for bulk and nano-$CuCl_2.2H_2O$ in distillate H_2O at 288.15, 293.15, 298.15, and 303.15 K.

Table 6: Gibbs free energy of association (ΔG_A), enthalpy change (ΔH_A), and entropy change (ΔS_A) for bulk and nano-$CuCl_2{\cdot}2H_2O$ in distillate H_2O at different temperatures.

T (K)	ΔG_A (kJ mol^{-1})		ΔH_A (kJ mol^{-1})		E_A (kJ mol^{-1})		ΔS_A (kJ mol^{-1}K^{-1})	
	Bulk	Nano	Bulk	Nano	Bulk	Nano	Bulk	Nano
288.15	−11.028	−9.322					−0.0496	−0.0904
293.15	−11.059	−9.828	−12.928	−22.918	3.60	3.72	−0.0487	−0.0842
298.15	−10.949	−9.501					−0.0477	−0.0824
303.15	−10.993	−8.924					−0.0468	−0.0807

complexes [57] on drawing the molar conductance (Λ_m) for bulk and nano-Cu-CFT complexes at different temperatures versus the molar ratio of metal to ligand $[M]/[L]$ concentrations, as shown in Figure 9.

The formation constants (K_f) for bulk and nano-Cu-CFT complexes were calculated for each type of complexes (1 : 2) and (1 : 1) (M : L) by using

$$M^{2+} + L \leftrightarrow ML^{2+},$$

$$K_f = \frac{\left[ML^{2+}\right]}{\left[M^{2+}\right][L]} = \frac{\Lambda_{M-}\Lambda_{obs}}{(\Lambda_{obs-}\Lambda_{ML})[L]}, \tag{20}$$

$$[L] = [L]_t - \left\{[M]_t \frac{\Lambda_{M-}\Lambda_{obs}}{(\Lambda_{M-}\Lambda_{ML})}\right\}, \tag{21}$$

where Λ_m is the limiting molar conductance of the bulk and nano-$CuCl_2.2H_2O$ alone, Λ_{obs} is the molar conductance of solution during titration, Λ_{ML} is the molar conductance of the complex, and $[L]$ is the CFT concentration.

The Gibbs free energies changes of formation (ΔG_f) for each stoichiometric complex were calculated [4] by using

$$\Delta G_f = -2.303RT \log K_f. \tag{22}$$

The obtained values (K_f) for bulk and nano-Cu-CFT complexes and their calculated ΔG_f values are presented in Tables 7 and 8.

By drawing the relation between log K_f and $1/T$, different lines were obtained indicating the formation of (1 : 2) and (1 : 1) ($M : L$) stoichiometric complexes, as shown in Figure 10.

From the relation between log K_f and $1/T$, ΔH_f can be calculated for each type of complexes, from the slope of each line which equals ($-\Delta H_f/2.303$ R). The entropy (ΔS_f) for bulk and nano-Cu-CFT complexes was calculated for each type of complexes (1 : 2) and (1 : 1) ($M : L$) by using

$$\Delta G_f = \Delta H_f - T\Delta S_f. \tag{23}$$

The calculated values of (ΔH_f) and (ΔS_f) for bulk and nano-Cu-CFT complexes are presented in Tables 9 and 10.

It was observed that inflections at (1 : 2) M/L proportion and (1 : 1) M/L indicating the formation of both stoichiometric complexes in the solutions. These types of stoichiometric complexes are formed as a result of the interaction of bulk or nano-$CuCl_2$ with CFT in distillate H_2O at different temperatures. The complex formation parameters for (1 : 1) complexes are greater than those of (1 : 2) complexes indicating more favorable complexes. Also, the complex formation parameters (K_f, ΔG_f) increased by increasing temperatures due to an increase in the kinetic energies. This trend was supported by entropies data which are greater for (1 : 1) M/L complexes than (1 : 2) M/L complexes.

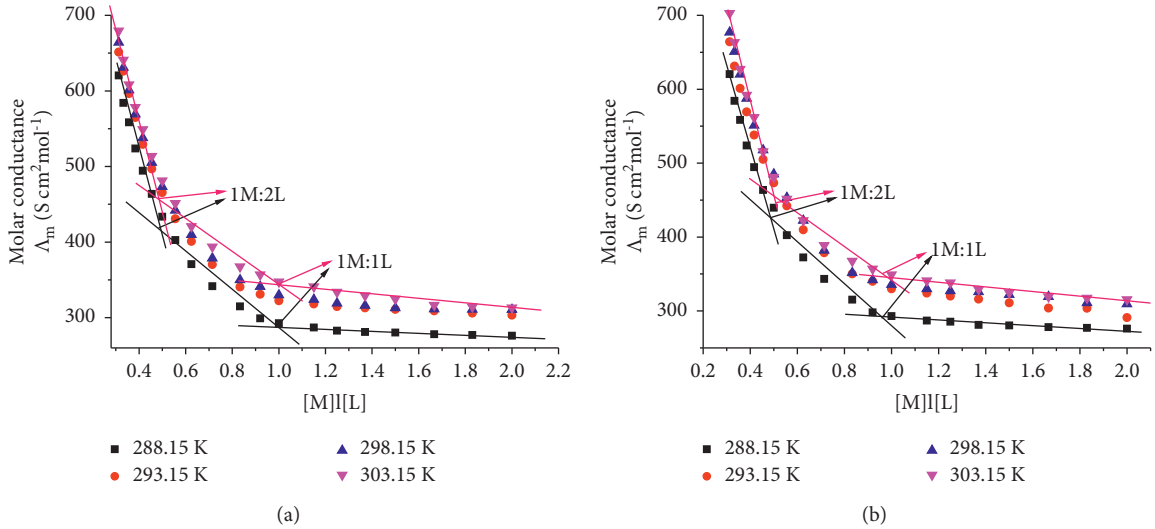

Figure 9: The relation between Λ_m and the [M]/[L] molar ratio for (a) bulk Cu-CFT complex and (b) nano-Cu-CFT complex in distillate H_2O at different temperatures.

Table 7: Limiting molar conductance (Λ_o) and formation constant (K_f) for bulk Cu-CFT complex in distillate H_2O at different temperatures.

T (K)	$[M]:[L]$	Λ_o S cm^2·mol^{-1}	Λ_{obs} S cm^2·mol^{-1}	log K_f dm^3·mol^{-1}
288.15	1 : 2	912.11	433.62	4.211
	1 : 1	554.03	440.05	4.424
293.15	1 : 2	958.50	473.22	4.186
	1 : 1	584.60	331.16	4.375
298.15	1 : 2	966.40	465.30	4.179
	1 : 1	594.50	322.25	4.342
303.15	1 : 2	985.30	481.14	4.174
	1 : 1	593.40	347.49	4.275

Table 8: Limiting molar conductance (Λ_o) and formation constant (K_f) for nano-Cu-CFT complex in distillate H_2O at different temperatures.

T (K)	$[M]:[L]$	Λ_o S cm^2·mol^{-1}	Λ_{obs} S cm^2·mol^{-1}	Log K_f dm^3·mol^{-1}
288.15	1 : 2	912.00	439.56	4.191
	1 : 1	555.00	290.00	4.426
293.15	1 : 2	966.00	473.22	4.177
	1 : 1	593.00	331.16	4.349
298.15	1 : 2	958.00	485.10	4.180
	1 : 1	584.00	335.61	4.323
303.15	1 : 2	985.30	481.14	4.171
	1 : 1	593.00	348.98	4.263

4. Biological Activity

Many transition metals show arresting biological activity, working as active centers within important bioactive molecules in living systems. Copper (II) plays a significant function in cell metabolism and has proved beneficial in numerous diseases [58–60]. Ceftriaxone-metal complexes have both pharmacological and toxicological properties [61]. The interaction between metal ions and ceftriaxone can lead to precipitation resulting in serious adverse drug events [62]. Ceftriaxone complexes have antibacterial properties that can decrease or increase relative to pure ceftriaxone [61]. The antimicrobial activity was estimated based on the size of the inhibition zone formed around discs of bulk $CuCl_2{\cdot}2H_2O$, nano-$CuCl_2{\cdot}2H_2O$, CFT, and its bulk and nano-Cu complexes on a petri dish with Luria Bertani agar (LB-agar) plates as it measures the compound's efficacy.

4.1. Antibacterial Activity. The antibacterial activities of bulk $CuCl_2.2H_2O$, nano-$CuCl_2{\cdot}2H_2O$, bulk and nano-Cu-CFT complexes were compared with the activity of CFT and as presented in Table 11. Bulk $CuCl_2{\cdot}2H_2O$ provides an excellent antimicrobial activity, and such property is greatly improved when using nano-$CuCl_2.2H_2O$. It was observed also that CFT has a higher zone of inhibition than bulk and nano-Cu-CFT complexes in *Klebsiella pneumonia* and *Pseudomonas aeruginosa* (gram-negative bacteria), Figure 11.

The antibacterial activity of Cu-CFT complexes depends on the bacterial species. The complexes and antibiotics presented inhibition zones of diameters larger than 20 mm showing that they have good activity as bactericides [63]. The antibacterial effect against *Staphylococcus aureus* is present at the bulk and nano-Cu-CFT complexes (the inhibition zones are 21 and 16 mm, respectively). These values are lower than the corresponding values for bulk $CuCl_2{\cdot}2H_2O$ and nano-$CuCl_2{\cdot}2H_2O$ and ceftriaxone. The data indicate that ceftriaxone ligand is more active than their metal complexes; this may be because the chelating ligands containing N and O donor atoms show wide biological activity through bonding to metal ions [64, 65]. However, the synergetic effects of ceftriaxone and Cu ion may play an important function in the inhibition of bacterial growth after the complex decomposition. These effects are due to the different mechanisms of the action of antibiotics and heavy ions on the bacteria metabolism [66, 67].

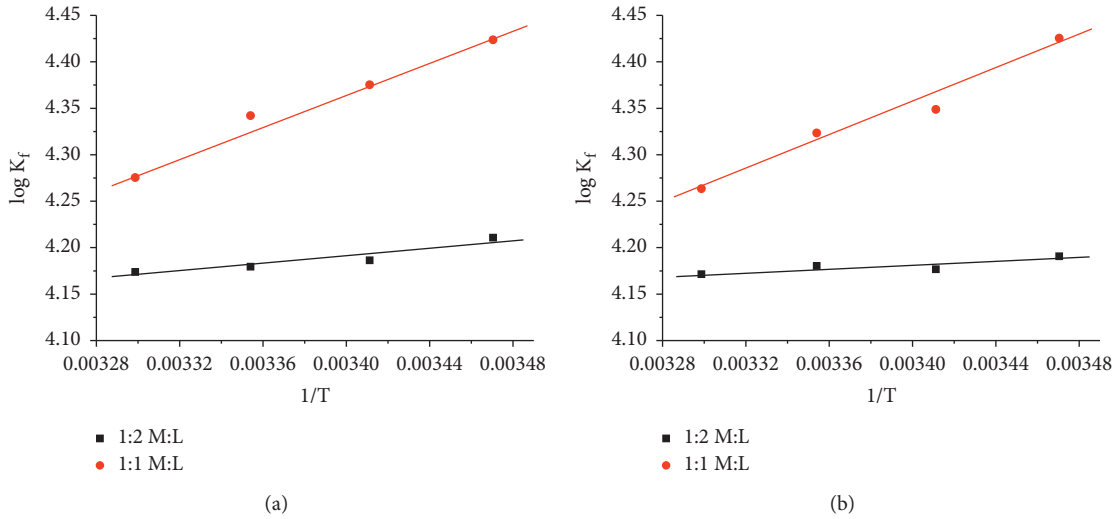

Figure 10: Variation of log K_f with l/T for (a) bulk Cu-CFT complex and (b) nano-Cu-CFT complex in distillate H_2O.

Table 9: Different formation parameters (Gibbs free energy of formation (ΔG_f), enthalpy change (ΔH_f), and entropy change (ΔS_f)) for bulk Cu-CFT complex in distillate H_2O at different temperatures.

T (K)	Complex ratio ($M:L$)	ΔG_f (kJ mol^{-1})	ΔH_f (kJ mol^{-1})	ΔS_f (kJ mol^{-1}K^{-1})
288.15	(1 : 2)	−23.23	−3.97	0.0252
293.15		−23.50		0.0257
298.15		−23.86		0.0265
303.15		−24.23		0.0273
288.15	(1 : 1)	−24.41	−15.96	0.0847
293.15		−24.56		0.0838
298.15		−24.79		0.0831
303.15		−24.82		0.0819

Table 10: Different formation parameters (Gibbs free energy of formation (ΔG_f), enthalpy change (ΔH_f), and entropy change (ΔS_f)) for nano-Cu-CFT complex in distillate H_2O at different temperatures.

T (K)	Complex ratio ($M:L$)	ΔG_f (kJ mol^{-1})	ΔH_f (kJ mol^{-1})	ΔS_f (kJ mol^{-1}K^{-1})
288.15	(1 : 2)	−23.12	−1.82	0.0208
293.15		−23.44		0.0215
298.15		−23.86		0.0226
303.15		−24.21		0.0234
288.15	(1 : 1)	−24.42	−17.13	0.0847
293.15		−24.41		0.0833
298.15		24.68		0.0828
303.15		−24.75		0.0816

Table 11: Inhibition zones for antibacterial activity (gram-negative bacteria) and antifungal activity (*Candida albicans*).

Compound	Inhibition zone (mm)		
	Types of gram-negative bacteria		Type of fungi
	Klebsiella pneumonia	*Staphylococcus aureus*	*Candida albicans*
Bulk $CuCl_2{\cdot}2H_2O$	19	17	12
Nano-$CuCl_2{\cdot}2H_2O$	23	22	14
Ceftriaxone (CFT)	34	33	0
Bulk Cu-CFT complex	24	21	8
Nano-Cu-CFT complex	25	16	9

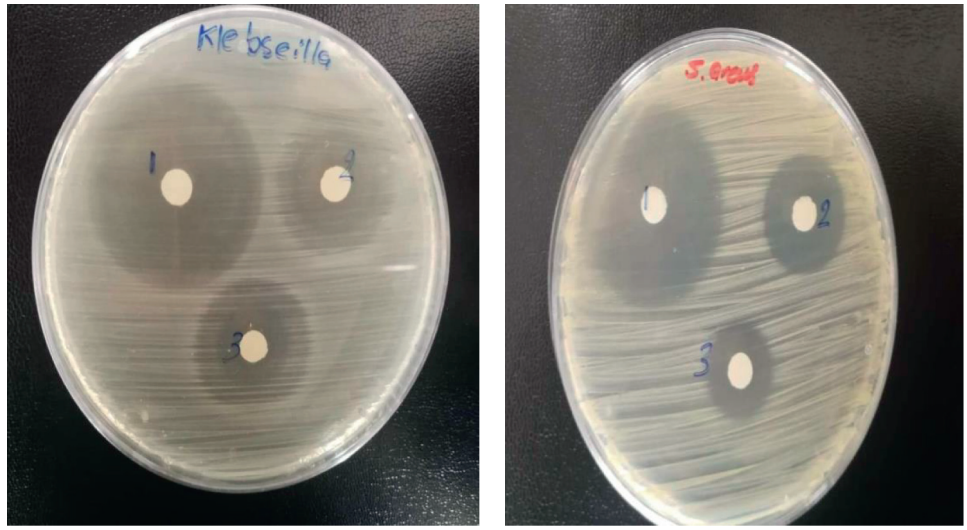

(a) (b)

Figure 11: Inhibition zone around the discs (6 mm) containing (1) CFT, (2) bulk Cu-CFT complex, and (3) nano-Cu-CFT complex placed on the surface of an LB-agar plate with (a) *Klebsiella pneumonia* and (b) *Pseudomonas aeruginosa.*

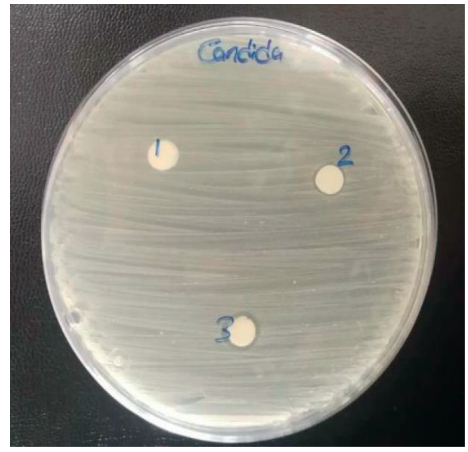

Figure 12: Inhibition zone around the discs (6 mm) containing (1) CFT, (2) bulk Cu-CFT complex, and (3) nano-Cu-CFT complex placed on the surface of an LB-agar plate with *Candida albicans* .

4.2. Antifungal Activity. The experimental antifungal activity data are presented in Table 11 which indicates that the nano-Cu-CFT complex showed a higher clear zone of inhibition against *Candida albicans* compared to the bulk Cu-CFT complex while there was an absence of the inhibition zone in CFT. So, the nano-Cu-CFT complex can be used as an antifungal drug, as shown in Figure 12. The zone of inhibition after treatment with bulk and nano-Cu-CFT complex was 8 and 9 mm, respectively. According to the standard criteria for evaluation of the drugs, the antifungal action such as a small zone of inhibition indicates that *Candida albicans* is stable with respect to CFT. The inhibition zones were completely absent, indicating the resistance of these fungi to CFT as well.

5. Conclusion

The nano-$CuCl_2{\cdot}2H_2O$ salt was prepared by ball milling method. The thermodynamic association parameters of both bulk and nano-$CuCl_2{\cdot}2H_2O$ salts in H_2O were calculated using the conductometric method by applying the Fuoss–Shedlovsky method at different temperatures. It shows that the association parameters of nano-$CuCl_2{\cdot}2H_2O$ are greater than bulk $CuCl_2{\cdot}2H_2O$ salt due to the high surface-to-volume ratio of the nanoparticles which leads to a greater ability for ion-pair formation.

The thermodynamic parameters of complexation between bulk and nano-$CuCl_2{\cdot}2H_2O$ salts and ceftriaxone antibiotic in H_2O were calculated from conductance measurement. It was found that the formation of Gibbs free

energies change (ΔG_f) was decreased in negative signs with increasing temperatures. Two stoichiometric complexes, 1/2 and 1/1 (M/L), are formed with the formation constant and Gibbs free energy of the formed complexes following the order $K_f\,(1:1) > K_f\,(1:2)$ for (M : L) and $\Delta G_f\,(1:1) > \Delta G_f\,(1:2)$ for ($M:L$) (in negative values) indicates the favorable of formation of (1 : 1) complex compared to (1 : 2) complex. Also, there is a decrease in values of K_f and ΔG_f in case of using nano-$CuCl_2{\cdot}2H_2O$ compared to using bulk $CuCl_2{\cdot}2H_2O$ but in small difference due to the more solvation effect in case of using nanoparticles.

It was observed that CFT has a higher zone of inhibition and antibacterial activity than that of bulk and nano-Cu-CFT complexes in *Klebsiella pneumonia* and *Pseudomonas aeruginosa* (gram-negative bacteria). The nano-Cu-CFT complex showed a higher clear zone of inhibition and antifungal activity against *candida* compared to the bulk Cu-CFT complex while there was an absence of the inhibition zone in CFT, so the nano-Cu-CFT complex can be used as an antifungal drug.

Data Availability

The data are available on request from the corresponding author.

Conflicts of Interest

The authors declare that there are no conflicts of interest regarding the publication of this paper.

Authors' Contributions

Elsayed M. AbouElleef conceptualized the study, supervised the study, wrote the original draft, reviewed and edited the article, developed the methodology, performed formal Analysis, performed data collection and analysis, performed investigation, performed visualization, and performed project administration. Mowafak M. Mahrouka performed investigation, developed the methodology, and wrote the manuscript. Sherine E. Salem performed data collection and analysis, provided the resources, performed investigation, and developed the methodology.

Acknowledgments

The authors gratefully acknowledge the approval and the support of this research study by from the Deanship of Scientific Research at Northern Border University Grant no. 8022-SAR-2018-3-9-F, Arar, KSA.

References

[1] J. D. Moore, J. P. Stegemeier, K. Bibby, S. M. Marinakos, G. V. Lowry, and K. B. Gregory, "Impacts of pristine and transformed Ag and Cu engineered nanomaterials on surficial sediment microbial communities appear short-lived," *Environmental Science and Technology*, vol. 50, no. 5, pp. 2641–2651, 2016.

[2] S. D. Nishu, S. Park, Y. Ji, I. Han, J. Key, and T. K. Lee, "The effect of engineered PLGA nanoparticles on nitrifying bacteria in the soil environment," *Journal of Industrial and Engineering Chemistry*, vol. 84, pp. 297–304, 2020.

[3] V. D. Chavada, N. M. Bhatt, M. Sanyal, and P. S. Shrivastav, "Citrate/melamine functionalized gold nanoparticles for concurrent determination of allopurinol and its major metabolite, oxypurinol in plasma and pharmaceuticals," *Journal of Industrial and Engineering Chemistry*, vol. 84, pp. 141–149, 2020.

[4] L. Narimani, M. Rezayi, W. P. Meng, and Y. Alias, "Measurements of thermodynamic parameters for complexation between a tetra-aza macrocycle ligand and some metal cations based on conductometric method," *Measurement*, vol. 77, pp. 362–372, 2016.

[5] J. N. Tiwari, R. N. Tiwari, and K. S. Kim, "Zero-dimensional, one-dimensional, two-dimensional and three-dimensional nanostructured materials for advanced electrochemical energy devices," *Progress in Materials Science*, vol. 57, no. 4, pp. 724–803, 2012.

[6] J. E. Lee, N. Lee, T. Kim, J. Kim, and T. Hyeon, "Multifunctional mesoporous silica nanocomposite nanoparticles for theranostic applications," *Accounts of Chemical Research*, vol. 44, no. 10, pp. 893–902, 2011.

[7] H. Barrak, T. Saied, P. Chevallier, G. Laroche, A. M'nif, and A. H. Hamzaoui, "Synthesis, characterization, and functionalization of ZnO nanoparticles by N-(trimethoxysilylpropyl) ethylenediamine triacetic acid (TMSEDTA): investigation of the interactions between phloroglucinol and ZnO@TMSEDTA," *Arabian Journal of Chemistry*, vol. 12, no. 8, pp. 4340–4347, 2019.

[8] M. Mansha, A. Qurashi, N. Ullah, F. O. Bakare, I. Khan, and Z. H. Yamani, "Synthesis of In2O3/graphene heterostructure and their hydrogen gas sensing properties," *Ceramics International*, vol. 42, no. 9, pp. 11490–11495, 2016.

[9] I. Rawal and A. Kaur, "Synthesis of mesoporous polypyrrole nanowires/nanoparticles for ammonia gas sensing application," *Sensors and Actuators A: Physical*, vol. 203, pp. 92–102, 2013.

[10] H. Ullah, I. Khan, Z. H. Yamani, and A. Qurashi, "Sonochemical-driven ultrafast facile synthesis of SnO2 nanoparticles: growth mechanism structural electrical and hydrogen gas sensing properties," *Ultrasonics Sonochemistry*, vol. 34, pp. 484–490, 2017.

[11] M. Ganesh, P. Hemalatha, M. M. Peng, and H. T. Jang, "One pot synthesized Li, Zr doped porous silica nanoparticle for low temperature CO_2 adsorption," *Arabian Journal of Chemistry*, vol. 10, pp. S1501–S1505, 2017.

[12] P. V. R. K. Ramacharyulu, R. Muhammad, J. Praveen Kumar, G. K. Prasad, and P. Mohanty, "Iron phthalocyanine modified mesoporous titania nanoparticles for photocatalytic activity and CO2 capture applications," *Physical Chemistry Chemical Physics*, vol. 17, no. 39, pp. 26456–26462, 2015.

[13] M. Shaalan, M. Saleh, M. El-Mahdy, and M. El-Matbouli, "Recent progress in applications of nanoparticles in fish medicine: a review," *Nanomedicine: Nanotechnology, Biology and Medicine*, vol. 12, no. 3, pp. 701–710, 2016.

[14] A. Astefanei, O. Núñez, and M. T. Galceran, "Characterisation and determination of fullerenes: a critical review," *Analytica Chimica Acta*, vol. 882, pp. 1–21, 2015.

[15] K. Saeed and I. Khan, "Preparation and characterization of single-walled carbon nanotube/nylon 6, 6 nanocomposites," *Instrumentation Science & Technology*, vol. 44, no. 4, pp. 435–444, 2016.

[16] K. Saeed and I. Khan, "Preparation and properties of single-walled carbon nanotubes/poly(butylene terephthalate)

nanocomposites," *Iranian Polymer Journal (English Edition)*, vol. 23, no. 1, pp. 53–58, 2014.

[17] J. M. Ngoy, N. Wagner, L. Riboldi, and O. Bolland, "A CO2 capture technology using multi-walled carbon nanotubes with polyaspartamide surfactant," *Energy Procedia*, vol. 63, pp. 2230–2248, 2014.

[18] P. G. Tratnyek and R. L. Johnson, "Nanotechnologies for environmental cleanup," *Nano Today*, vol. 1, no. 2, pp. 44–48, 2006.

[19] N. C. Mueller and B. Nowack, "Exposure modeling of engineered nanoparticles in the environment," *Environmental Science and Technology*, vol. 42, no. 12, pp. 4447–4453, 2008.

[20] E. C. Dreaden, A. M. Alkilany, X. Huang, C. J. Murphy, and M. A. El-Sayed, "The golden age: gold nanoparticles for biomedicine," *Chemical Society Reviews*, vol. 41, no. 7, pp. 2740–2779, 2012.

[21] E. T. Helmy, E. M. Abouellef, U. A. Soliman, and J. H. Pan, "Novel green synthesis of S-doped TiO2 nanoparticles using Malva parviflora plant extract and their photocatalytic, antimicrobial and antioxidant activities under sunlight illumination," *Chemosphere*, vol. 271, Article ID 129524, 2021.

[22] S. Alemayehu, T. Admasu, F. Mamo et al., "Evaluation of ceftriaxone utilization in medical and emergency wards of TikurAnbessa specialized hospital: a prospective cross sectional study," *BMC Pharmacology*, vol. 17, p. 7, 2016.

[23] F. A. Abebe, D. F. Berhe, A. H. Berhe et al., "Drug use evaluation of ceftriaxone: the case of ayder referral hospital, mekelle, Ethiopia," *International Journal of Pharmaceutical Sciences and Research*, vol. 3, pp. 2191–2195, 2012.

[24] E. Hedlund, "The protective effects of beta-lactam antibiotics in motor neuron disorders," *Experimental Neurology*, vol. 231, no. 1, pp. 14–18, 2011.

[25] D. A. Raja, S. G. Musharraf, M. R. Shah, A. Jabbar, and M. I. Bhanger, "Poly(propylene glycol) stabilized gold nanoparticles: an efficient colorimetric assay for ceftriaxone," *Journal of Industrial and Engineering Chemistry*, 2020.

[26] E. M. AbouElleef, M. N. Abd El-Hady, E. A. Gomaa, and A. G. Al-Harazie, "Conductometric association parameters for CdBr2 in the presence and absence of Ceftazidime in water and 30% ethanol–water mixtures," *Journal of Chemical & Engineering Data*, vol. 66, no. 2, pp. 878–889, 2021.

[27] E. M. AbouElleef and S. D. Mekkey, "Study of the thermodynamic parameters for interaction of ciprofloxacin antibiotic with bulk and nanocopper sulfate," *Journal of Biochemical Technology*, vol. 10, no. 1, pp. 57–66, 2019.

[28] G. H. Rounaghi, M. Mohajeri, S. Ahmadzadeh, and S. Tarahomi, "A thermodynamic study of interaction of Na+ cation with benzo-15-crown-5 in binary mixed non-aqueous solvents," *Journal of Inclusion Phenomena and Macrocyclic Chemistry*, vol. 63, no. 3-4, pp. 365–372, 2009.

[29] S. Ahmadzadeh, M. Rezayi, E. Faghih-Mirzaei, M. Yoosefian, and A. Kassim, "Highly selective detection of titanium (III) in industrial waste water samples using meso-octamethylcalix[4] pyrrole-doped PVC membrane ion-selective electrode," *Electrochimica Acta*, vol. 178, pp. 580–589, 2015.

[30] S. Ahmadzadeh, M. Rezayi, H. Karimi-Maleh, and Y. Alias, "Conductometric measurements of complexation study between 4-Isopropylcalix[4]arene and Cr3+ cation in THF-DMSO binary solvents," *Measurement*, vol. 70, pp. 214–224, 2015.

[31] S. Ahmadzadeh, M. Yoosefian, and M. Rezayi, "Comprehensive experimental and theoretical investigations on chromium (III) trace detection in biological and environmental samples using polymeric membrane sensor," *International Journal of Environmental Analytical Chemistry*, pp. 1–16, 2019.

[32] S. Badakhshan, S. Ahmadzadeh, A. Mohseni-Bandpei, M. Aghasi, and A. Basiri, "Potentiometric sensor for iron (III) quantitative determination: experimental and computational approaches," *BMC Chemistry*, vol. 13, no. 1, p. 131, 2019.

[33] S. Santra and B. Das, "Counterion-binding and related phenomena in sodium alginate-sodium chloride-water ternary systems: a conductometric study," *Journal of Molecular Liquids*, vol. 296, p. 111930, 2019.

[34] P. Scherrer, *Nachrichten von der Gesellschaft der Wissenschaften zu Gittingen, Mathematisch-Physikalische Klasse*, vol. 26, no. 1, pp. 98–100, Jul. 1918.

[35] Y. Waseda, E. Matsubara, and K. Shinoda, *X-ray Diffraction Crystallography: Introduction, Examples and Solved Problems*, Springer, Berlin, Germany, 2011.

[36] D. Harker, "The crystal structure of cupric chloride dihydrate $CuCl_2 \cdot 2H_2O$," *Zeitschrift für Kristallographie - Crystalline Materials*, vol. 93, no. 1-6, pp. 136–145, 1936.

[37] A. Umer, S. Naveed, N. Ramzan, M. Rafique, and M. Imran, "A green method for the synthesis of Copper Nanoparticles using L-ascorbic acid," *Matéria (Rio de Janeiro)*, vol. 19, no. 3, pp. 197–203, 2014.

[38] R. A. Nyquist, "α-Halo-*p*-X-substituted acetanilides: effects on the N-H and C=O stretching frequencies and intensities in dilute solution," *Spectrochimica Acta*, vol. 19, no. 9, pp. 1595–1605, 1963.

[39] M. Mashima, "Infrared absorption spectra of hydrazides. I. Hydrazides of aromatic acidsþ," *Bulletin of the Chemical Society of Japan*, vol. 35, no. 332, p. 1862, 1962.

[40] H. J. Bernstein, "The average XH stretching frequency as a measure of XH bond properties," *Spectrochimica Acta*, vol. 18, no. 2, pp. 161–170, 1962.

[41] A. Marco, *Compt. Rend.*vol. 274B, p. 400, 1972.

[42] A. Tramer, "N° 25. - spectres de vibration et structure des sulfocyanures complexes," *Journal de Chimie Physique*, vol. 59, pp. 232–240, 1962.

[43] J. Chouteau, G. Davidovics, J. Metzger, and A. Bonzom, "Sur le spectre infrarouge de l'amino-2 thiazole, du méthyl-4 amino-2 thiazole et de leurs dérivés NN dialcoylés—II," *Etude á l'état liquide—Essai d'interprétation générale.cccSpectrochimica Acta*, vol. 22, no. 4, pp. 719–735, 1966.

[44] M. Oki and M. Hirota, "Intramolecular hydrogen bonding in α-keto-and α-alkoxy-carboxylic acids. VI. substituent effects on the energy of the hydrogen bonding in α-alkoxy-and α-alkoxy-and α-aryloxyacetic acids," *Bulletin of the Chemical Society of Japan*, vol. 36, p. 290, 1963.

[45] A. S. Gilbert, A. M. North, T. G. Parker, and R. A. Pethrick, "Submillimetre and far i.r. studies of normal and branched chain hydrocarbons," *Spectrochimica Acta Part A: Molecular Spectroscopy*, vol. 32, no. 5, pp. 931–936, 1976.

[46] A. J. Abdulghani and S. K. Mohuee, "Synthesis and characterization of new schiff bases derived from ceftriaxone sodium with 1H- indole-2, 3- dione (isatin) and 1-acetyl indoline-2, 3-dione (NAcetylisatin) and their platinum (IV) complexes," *Journal of Chemical, Biological and Physical Sciences*, vol. 6, pp. 579–595, 2016.

[47] A. J. Abdulghani and R. K. Hussain, "Synthesis and characterization of schiff base metal complexes derived from cefotaxime with 1H-indole-2,3-dione (isatin) and 4-N,N-dimethyl-aminobenzaldehyde," *Open Journal of Inorganic Chemistry*, vol. 05, no. 04, pp. 83–101, 2015.

[48] E. A. Gomaa, E. M. AbouElleef, K. S. Shalaby, and S. E. Salem, "Thermodynamic effect of bulk and nano-CuCl2 salts on

tenoxicam using a variety of different techniques," *Journal of Forestry and Environment*, vol. 1, pp. 44–53, 2014.

[49] E. T. Helmy, E. A. Gomaa, and E. M. AbouElleef, "Complexation of 2-mercaptoimidazol with some barium salts conductometrically in various solvents at different temperatures," *Int. J. Mod. Chem.*vol. 7, pp. 141–155, 2015.

[50] G. Kumar and M. S. Chauhan, "Conductometric investigations of surfactant behavior in aqueous polar aprotic organic additives," *Journal of Molecular Liquids*, vol. 249, pp. 710–715, 2018.

[51] A. A. Khan, M. Q. Khan, and R. Hussain, "Determination of Cu2+ in aqueous solution using a polyindole-tin(IV) molybdophosphate conductive nanocomposite ion-selective membrane electrode," *Journal of Physics and Chemistry of Solids*, vol. 123, pp. 113–123, 2018.

[52] S. Das, D. Ekka, and M. Roy, "Conductance and FTIR spectroscopic study of triple-ion formation of tetrabutylphosphonium methanesulfonate in methylamine solution," *Chemical Methodologies*, vol. 4, no. 1, pp. 55–67, 2020.

[53] E. A. Gomaa, E. M. AbouElleef, and E. T. Helmy, "Conductance studies on complex formation between CaCl2 and ampicillin as ligand in water and in methanol solvent at different temperatures," *RRJPPS*, vol. 3, pp. 55–64, 2014.

[54] E. A Gomaa and R. Tarek Rashad, "Determination of thermodynamic parameters of VOSO4 in different organic mixed solvents," *Chemical Sciences Journal*, vol. 09, no. 02, p. 187, 2018.

[55] E. AbouElleef and E. Helmy, "Antibiotic oxytetracycline solvation Inter⌓ctions with ethanol-aqueous mixturs at different temperatures," *Egyptian Journal of Chemistry*, vol. 63, no. 2, pp. 499–506, 2020.

[56] E. A. Gomaa, A. Negm, and M. A. Tahoon, "Conductometric and volumetric study of copper sulphate in aqueous ethanol solutions at different temperatures," *Journal of Taibah University for Science*, vol. 11, no. 5, pp. 741–748, 2017.

[57] M. Biedulska, A. Chylewska, and D. Nidzworski, "Comparative solution equilibria studies of complex formation between Ir(III) ion and antituberculosis drug analogues: spectroscopic, potentiometric and conductometric approach," *Journal of Molecular Liquids*, vol. 296, Article ID 111887, 2019.

[58] D. R. Williams, *The Metals of Life*, Van Nostrand Reinhold, London, 1971.

[59] D. H. Brown, W. E. Smith, J. W. Teape, and A. J. Lewis, "Antiinflammatory effects of some copper complexes," *Journal of Medicinal Chemistry*, vol. 23, no. 7, pp. 729–734, 1980.

[60] J. R. J. Sorenson, *Copper in the Environment*Wiley-Interscience, New York, NY, USA, 1981.

[61] J. R. Anacona and A. Rodriguez, "Synthesis and antibacterial activity of ceftriaxone metal complexes," *Transition Metal Chemistry*, vol. 30, no. 7, pp. 897–901, 2005.

[62] H.-R. Schmutz, P. Detampel, T. Bühler, A. Büttler, B. Gygax, and J. Huwyler, "In vitro assessment of the formation of ceftriaxone-calcium precipitates in human plasma," *Journal of Pharmaceutical Sciences*, vol. 100, no. 6, pp. 2300–2310, 2011.

[63] D. L. Shungu, E. Weinberg, and H. H. Gadebusch, "Tentative interpretive standards for disk diffusion susceptibility testing with norfloxacin (MK-0366, AM-715)," *Antimicrobial Agents and Chemotherapy*, vol. 23, no. 2, pp. 256–260, 1983.

[64] R. C. Maurya, P. Patel, and S. Rajput, "Synthesis and characterization of N-(o-Vanillinidene)-p-anisidine and N,N′-bis(o-Vanillinidene)ethylenediamine and their metal complexes," *Synthesis and Reactivity in Inorganic and Metal-Organic Chemistry*, vol. 33, no. 5, pp. 817–836, 2003.

[65] U. Bohme and B. Gunther, *Inorganic Chemistry Communications*, vol. 10, pp. 482–484, 2007.

[66] L. Peng, R. Lifang, X. Hongyu, L. Xi, and Z. Chaocan, "Study on the toxic effect of lead(II) ion on *Escherichia coli*," *Biological Trace Element Research*, vol. 115, no. 2, pp. 195–202, 2007.

[67] A. Yotsuji, J. Mitsuyama, R. Hori et al., "Outer membrane permeation of Bacteroides fragilis by cephalosporins," *Antimicrobial Agents and Chemotherapy*, vol. 32, no. 7, pp. 1097–1099, 1988.